Tribol Lett (2015) 59:1
DOI 10.1007/s11249-015-0539-9

METHODS PAPER

A Technique for the Experimental Determination of the Length and Strength of Adhesive Interactions Between Effectively Rigid Materials

Tevis D. B. Jacobs[1] · Joel A. Lefever[2] · Robert W. Carpick[3]

Received: 23 March 2015 / Accepted: 20 April 2015

Abstract To describe adhesion between bodies of known arbitrary shape and known elastic properties, contact mechanics models require knowledge or assumptions of a minimum of two parameters, the strength of the adhesive interaction (characterized by the intrinsic work of adhesion $W_{\text{adh,int}}$) and the length scale of the interaction (described by the range of adhesion z_0). One parameter can easily be measured if the other is estimated or assumed, but experimental techniques for determining both simultaneously are lacking. Here, we demonstrate a novel technique—called the Snap-in/pull-off Numerical Adhesion Parameter method—for experimentally determining both parameters simultaneously using adhesion measurements performed with an atomic force microscope probe whose geometry has been characterized. The method applies to materials that approach the rigid limit (high elastic moduli). The technique is explained and validated analytically for simple shapes (flat punch, paraboloid, and right cone), and trends in results are compared against prior literature. This approach allows calculation of the adhesion parameters to enable prediction of adhesion behavior, including for advanced technology applications.

Keywords Adhesion · Nanoscale · Work of adhesion · Range of adhesion AFM · TEM

✉ Tevis D. B. Jacobs
tjacobs@pitt.edu

✉ Robert W. Carpick
carpick@seas.upenn.edu

[1] Department of Mechanical Engineering and Materials Science, University of Pittsburgh, 538-E Benedum Hall, 3700 O'Hara St., Pittsburgh, PA 15261, USA

[2] Department of Materials Science and Engineering, University of Pennsylvania, 3231 Walnut St., Philadelphia, PA 19104, USA

[3] Department of Mechanical Engineering and Applied Mechanics, University of Pennsylvania, 229 Towne Bldg, 220 S. 33rd St., Philadelphia, PA 19104, USA

1 Introduction

The fundamental physics governing adhesion are well understood; however, the direct measurement of adhesive parameters between two surfaces remains difficult, especially when surfaces are not simply shaped (e.g., smooth spheres or planes). Yet accurate knowledge of adhesion between technologically relevant surfaces is critical for research, development, and commercialization of nanoscale devices.

1.1 Mathematical Parameters Describing Adhesion Between Planar Surfaces

The work of adhesion W_{adh} between two surfaces is the energy per unit area required to separate two planar surfaces from equilibrium contact to infinite separation. It is defined as:

$$W_{\text{adh}} = \left(\gamma_i + \gamma_j\right) - \gamma_{ij}, \tag{1}$$

where γ_i is the surface energy of surface i and γ_{ij} is the interfacial energy between surfaces i and j. In accordance with prior literature on adhesion and roughness [1], the *intrinsic* work of adhesion $W_{\text{adh,int}}$ is the work of adhesion between perfectly flat, planar surfaces. While $W_{\text{adh,int}}$ is a continuum concept, it maps robustly onto an atomistic description of a perfectly flat, single crystal surface. The

Published online: 20 May 2015

effective work of adhesion $W_{adh,eff}$ is defined as the work of adhesion for the same material pair in the case where one or both planar surfaces contain local surface roughness. The distinction between $W_{adh,int}$ and $W_{adh,eff}$ is shown schematically in Fig. 1. The $W_{adh,int}$ is determined by the identity of the materials in contact and the environment, whereas $W_{adh,eff}$ is a function of $W_{adh,int}$ and the local surface topography. For hard, nonconforming materials, $W_{adh,eff}$ is typically much smaller than $W_{adh,int}$ because the roughness increases the effective separation between the materials and decreases their area of intimate contact. This increased separation makes the interfacial energy γ_{ij} larger (i.e., the interface is less energetically favorable since the roughness prevents it from adopting a more favorable state of intimate bonding). This distinction is drawn because many experimental techniques exist to measure $W_{adh,eff}$ (for example, using microfabricated beam tests [2]), but generally applicable techniques to deduce the $W_{adh,int}$ do not exist. The latter quantity $W_{adh,int}$ is required for the prediction of adhesion in a particular scientific or technological application. Therefore, this paper offers an experimental method for determining $W_{adh,int}$ for stiff, nonconforming materials.

Further, while knowledge of $W_{adh,int}$ is useful, it is insufficient for prediction of adhesive force given an arbitrary contact geometry. Rather, a complete description of adhesion using continuum contact mechanics requires—at a minimum—knowledge of two parameters that describe the force–separation interaction of the materials: the strength of adhesion, such as $W_{adh,int}$; and the length scale of adhesion, such as z_0. Physically, z_0 describes the equilibrium separation distance between perfectly flat surfaces, i.e., the separation distance at which their interaction force is zero. When only two parameters are used to describe the adhesive interaction, z_0 will also describe the length scale of the interaction. Accordingly, in many mathematical descriptions of adhesion (for instance, Refs. [3–6]), z_0 is presented and used as the governing parameter to scale the distance over which adhesion acts for a particular material. Therefore, the parameter z_0 is referred to in this paper as the "range of adhesion," (in accordance with J. A. Greenwood [3], who calls it the "range of action of the surface forces"). When combined with knowledge of the shape and elastic properties of the bodies, a complete description of the contact mechanics behavior (pull-off force, contact area, contact displacement, and contact stresses vs. applied load) can be determined.

Other mathematical descriptions of adhesion use different variables, but still contain independent parameters describing a strength of adhesion and a length scale, e.g., ε and σ in Eq. 7.6 of [7] for Lennard–Jones, or A and D_0 in Eq. 13.37 of [7] for a van der Waals interaction with a cutoff, or $W_{adh,int}$ and h in [8]. In all cases, the two parameters from one description can be written in terms of the two from another; $W_{adh,int}$ and z_0 have been written in terms of ε and σ in [7], in terms of A and D_0 in [7], and in terms of $W_{adh,int}$ and h in [4]. It has been shown [9, 10] that the adhesion between realistic shapes depends primarily on choice of parameters and only secondarily on the exact form of the model. The work on adhesion and roughness by Persson et al. [1] requires only one parameter, $W_{adh,int}$, but assumes that all adhesion is taking place *at* the contact interface, with no adhesive interaction for material that is near to contact, but not touching (equivalent to the JKR limit of contact [8]). Their method can be generalized to materials outside of this limit, but requires an additional description of interaction forces at nonzero separation and thus knowledge of the length scale of these interactions (as discussed in [11]). Further, their method applies only to surfaces with self-affine topography. In summary, while the present paper uses the specific adhesive framework of Greenwood [3] and others [4–6], the results can be generalized to measure the relevant parameters required for other mathematical two-parameter treatments of adhesion.

1.2 Contact Mechanics Models Describing Adhesion Between Arbitrarily Shaped Surfaces

The adhesion models described above can all be generalized to predict the adhesive force between bodies of arbitrary shape. For the special case of adhesive spheres under limiting case conditions, only $W_{adh,int}$ is required [12]. For example,

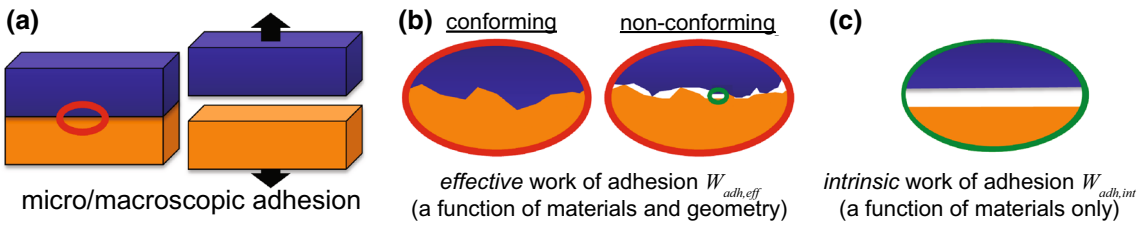

Fig. 1 Intrinsic and effective works of adhesion can differ significantly. A micro/macroscopic adhesion test (**a**) typically measures an effective value, due to roughness of the contact (**b**). The intrinsic work of adhesion describes contact between perfectly flat surfaces (**c**) and is therefore determined by the materials in contact

stiff spheres with long-range adhesion (essentially, z_0 is infinite) are described by the famous Derjaguin–Müller–Toporov (DMT) model and compliant spheres with short-range adhesion ($z_0 = 0$) are described by the Johnson–Kendall–Roberts (JKR) model. But even in these cases, the z_0 parameter is required to determine the appropriate limit. Further, in the more general case of bodies with nonspherical shapes [13] or spheres that do not fall into one of the limiting cases [8], knowledge of both $W_{\text{adh,int}}$ and z_0 is explicitly required.

Specifically, adhesion in these more general cases is mathematically described using a traction–separation relation for two materials, which defines the adhesive stress (force per unit area) between two flat surfaces as a function of separation distance. Under the Derjaguin approximation (discussed in more detail in [3]), the adhesion force between two bodies of arbitrary shape can be calculated by integrating this traction–separation relation over the geometry of the contact.

One traction–separation relation in common use [3–6] is the Lennard–Jones surface interaction. For two semi-infinite parallel surfaces separated by a distance z, the normal stress σ_{normal} acting between the two surfaces is written in the following form [3]:

$$\sigma_{\text{normal}}(z) = \frac{F_{\text{surf}}}{A_{\text{surf}}} = -\frac{8W_{\text{adh,int}}}{3z_0}\left[\left(\frac{z_0}{z}\right)^3 - \left(\frac{z_0}{z}\right)^9\right] \tag{2}$$

where F_{surf} is the total load acting on surfaces of area A_{surf}, and the shape of the traction–separation relation is governed by $W_{\text{adh,int}}$ and z_0. This Lennard–Jones traction–separation relation can be derived by integrating the Lennard–Jones interatomic potential over a flat surface [14]. Note that the attractive term ($\sim z^{-3}$) is derived from van der Waals attraction, which is the primary attractive force in many technologically relevant systems (conductive and electronically neutral materials in dry environments under low applied loads). The repulsive term ($\sim z^{-9}$) derives from an empirical approximation to account for Pauli and electrostatic repulsion of surface electrons. As discussed, the adhesive force depends primarily on choice of $W_{\text{adh,int}}$ and z_0 and only secondarily on the specific traction–separation relation chosen [9, 10], so the present technique should be generalizable.

1.3 Experimental Difficulties Involved in Measuring Intrinsic Adhesion Properties

Despite the importance of accurate knowledge of $W_{\text{adh,int}}$ and z_0, these parameters are difficult to simultaneously measure experimentally. While pull-off forces can easily be measured—for instance by using an atomic force microscope (AFM)—it is normally not possible to extract both $W_{\text{adh,int}}$ and z_0 solely from this measurement. One approach is to modify the AFM [15–18] or use other instruments like the Interfacial Force Microscope to avoid snap-in [19]. However, if tip shape is not measured then only effective values can be measured using these techniques. A typical approach is to assume that the apex of the AFM tip is a sphere of known radius R_{tip}; and then to apply adhesive-sphere contact mechanics (such as the DMT, JKR or Maugis models [8]) to extract a work of adhesion (this method is described in Ref. [20]). However, this approach requires assuming or otherwise determining the length scale of the adhesive interaction in order to select an appropriate contact model (as discussed in [8]). Furthermore, this approach is highly sensitive to errors in tip radius estimation. For nonspherical bodies, (such as those described by high-order power-law shapes) the pull-off force will also depend strongly on both $W_{\text{adh,int}}$ and z_0 [13]. Therefore, to investigate adhesion using an experimental measurement of pull-off force, it is necessary to *assume* a value for one variable (usually z_0) and then solve for the value of the other ($W_{\text{adh,int}}$). The measured value of $W_{\text{adh,int}}$ is only as reliable as the assumption of z_0. It is common in contact mechanics literature to approximate z_0 based on intuition and order of magnitude arguments [21–23]. Further, a wide range of values for z_0 have been proposed or measured in previous literature, ranging from 0.15 [20] to 5 nm [5]. The present technique is proposed for experimentally measuring both adhesion parameters simultaneously, in order to accurately establish these heretofore-undetermined quantities.

1.4 Summary of the SNAP Method and the Structure of this Paper

The Snap-in/pull-off Numerical Adhesion Parameter method (or SNAP method) enables simultaneous determination of $W_{\text{adh,int}}$ and z_0, using geometrical characterization of an AFM tip, coupled with adhesion measurements using the same tip. More specifically, three measurements are taken for a tip/sample pair: (1) the pull-off force; (2) the snap-in distance; and (3) the fine-scale shape of the AFM tip. Then, a traction separation law can be integrated over the measured geometry with $W_{\text{adh,int}}$ and z_0 as fitting parameters. These parameters are adjusted until the calculated values for pull-off force and snap-in distance match the measured values. The technique is valid for measuring adhesion between any hard, nonconforming materials. The novel aspects of this technique are: (a) the use of measured tip geometry instead of the assumption of a shape that matches an analytical function (sphere, flat punch, etc.) and (b) the use of the snap-in distance as an additional data point to enable simultaneous extraction of z_0.

The structure of the present article is as follows—Sect. 2 describes general ways of determining tip shape,

snap-in distance, and pull-off force (the needed inputs to calculate adhesion parameters). Section 3 discusses the mathematical framework for extracting $W_{adh,int}$ and z_0 using these inputs, including an illustrative example. In Sect. 4, a validation of this method is presented, where adhesion parameters are calculated and back-calculated for simple, geometric shapes (a flat punch, a paraboloid, and a right cone); this ensures self-consistency, assesses self-consistency of the technique, and allows comparison against trends in previous literature. The final section presents concluding remarks. Application of the present technique to in situ experimental data is presented elsewhere [24].

2 Technique for Determining Tip Geometry and Adhesion Measurements

Several methods exist for characterizing the geometry of an AFM tip, for instance: direct imaging using electron microscopy; direct imaging of the tip apex in an AFM using a sharper AFM tip; tip reconstruction algorithms that extract tip shape from AFM scans of a known surface; and destructive characterization (after adhesion testing) using atom probe tomography. The present technique can be applied regardless of how the AFM tip geometry is measured; however, we suggest that characterization using high-resolution TEM represents the best combination of ease and reliability. In particular, the AFM chip can be mounted in the TEM using simple custom fixtures, as was done in [25]. The apex of the tip can be characterized as shown in Fig. 2a. Then, the two-dimensional outer contour of the probe's profile can be identified using contrast differences in the TEM, as shown in Fig. 2b, for instance, by using edge-finding software routines. A drawback of the TEM method is that the three-dimensional tip shape is not resolved, only a 2D profile. Using a goniometer or a tilting stage can partially but not fully address this. Thus, for this work, we create a three-dimensional shape (Fig. 2c) from a two-dimensional contour by assuming the tip has a circular profile at each resolved height increment. Note that this does not assume global axisymmetry about a single axis of rotation (as is true for a right cone), but rather assumes local axisymmetry, with the potential for different axes of rotation at different locations along the height (z-axis). It further assumes that the probe is free of debris (which is readily observed), and that the axis of the probe is pointing downward (which is accomplished by rotating the 2D profile prior to the analysis). For the tip shown in Fig. 2 and several other tips, TEM images taken at a variety of tilt angles inside the TEM consistently demonstrate that the assumption of circular cross section is reasonable over the apex region of the tip where the adhesion forces are acting,

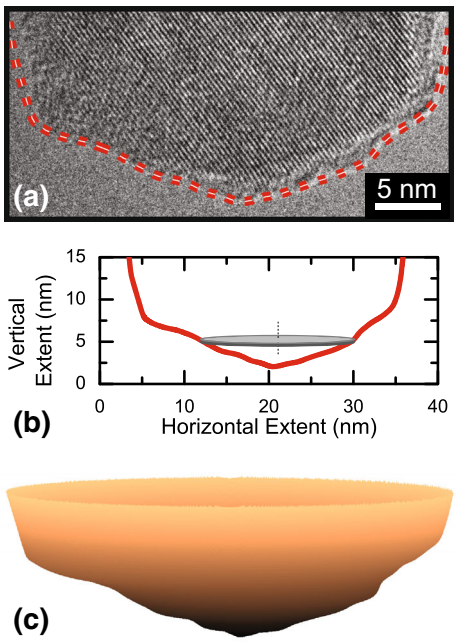

Fig. 2 Lattice-resolved images of AFM tips (**a**) can be obtained using a transmission electron microscope. The apex of the tip can then be traced (manually, or using image processing routines) to yield its outer profile (*red line*). The two-dimensional profiles were integrated using a method of disks (**b**) to create a three-dimensional shape (**c**), from which the interaction was calculated (Color figure online)

except in cases where debris is visible or immediately after a large fracture event has occurred along a defined crystallographic plane. This has been confirmed in another study [26] by comparing TEM images to tip shapes determined through AFM scans using numerical tip reconstruction algorithms. In the case of multiple protrusions on the end of the tip, this assumption of local axisymmetry is assumed to apply separately to each.

Once the AFM probe has been characterized, adhesion tests are conducted using methods common in atomic force microscopy [27], as shown in Fig. 3. These adhesion tests provide two independent pieces of information about the force of interaction between the tip and sample. First, the measured pull-off force ($F_{pull\text{-}off}$) yields the maximum attractive force that occurs between the two bodies. Second, the measured snap-in distance ($d_{snap\text{-}in}$) yields the gradient of the force–distance curve at a known separation distance. In particular, the snap-in event (well known in AFM) occurs when the gradient of the interaction force between the two surfaces exceeds the spring constant k_{lever} of the cantilever [27]. At larger separation distances, instantaneous fluctuations in separation are damped out by the restoring force of the cantilever (stable equilibrium). The snap-in point represents the transition to unstable equilibrium, where slight perturbations in separation lead to a reduction in system energy and cause the tip to accelerate irreversibly

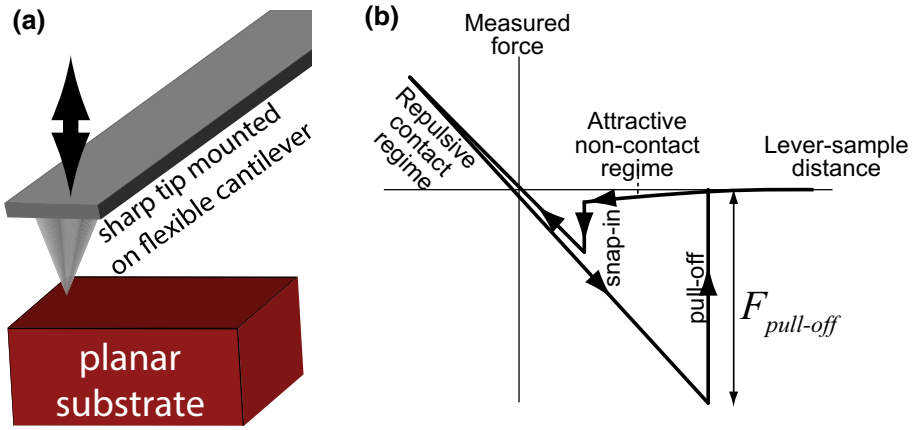

Fig. 3 Pull-off force and snap-in distance can be easily obtained using a standard atomic force microscope (AFM), a schematic of which is shown in (**a**). A canonical force curve is shown in (**b**), including the magnitude of the pull-off force $F_{\text{pull-off}}$. By dividing the force change at snap-in by the cantilever spring constant, the snap-in distance $d_{\text{snap-in}}$ can be calculated

toward the surface. Thus, if k_{lever} is known, then the gradient of the tip/sample interaction force (equal to the spring constant of the cantilever) is known at a separation distance equal to $d_{\text{snap-in}}$. Where possible, the adhesion parameters should be measured multiple times and averaged. Thermal fluctuations, instrumental drift, and local variations in the substrate surface can cause variability in the measured quantities. Rate-dependence of pull-off and viscoelasticity play a large role for softer contacts, but are not as important for stiff contacts.

3 Mathematical Technique for Determining Adhesion Parameters

The two values ($F_{\text{pull-off}}$ and $d_{\text{snap-in}}$) measured in the adhesion test provide two independent pieces of information about the interaction between the tip and sample: the maximum attractive force and the gradient of the interaction at a specific tip-sample separation distance. For a given tip geometry, if $W_{\text{adh,int}}$ and z_0 are known then $F_{\text{pull-off}}$ and $d_{\text{snap-in}}$ can be calculated—as discussed in Sect. 3.1. Alternatively (and more commonly), if $F_{\text{pull-off}}$ and $d_{\text{snap-in}}$ are known, then $W_{\text{adh,int}}$ and z_0 can be calculated—as discussed in Sect. 3.2.

3.1 Calculating $F_{\text{pull-off}}$ and $d_{\text{snap-in}}$ from Known Values of $W_{\text{adh,int}}$ and z_0

The adhesive force $F_{\text{tip/sample}}$ is calculated at many different values of tip/sample separation distance d by breaking the tip into differential elements of surface, as shown schematically in Fig. 4a, and using the Lennard–Jones 3–9 traction–separation relation (Eq. 2) to calculate adhesive stress on every element. The element/element separation is $z_{\text{sep}} = z_{\text{tip}} + d$, where z_{tip} is the local height of that element; the contribution from all differential elements is summed to yield the total interaction force. Numerically, this is calculated as follows:

$$F_{\text{tip/sample}} = \int_{\text{Area}} \sigma_{\text{normal}}(z_{\text{sep}})\mathrm{d}A = \int_0^{2\pi}\int_0^{\infty} \sigma_{\text{normal}}(z_{\text{sep}}(r,\theta))r\mathrm{d}r\mathrm{d}\theta = \int_0^{\infty}\left\{\frac{8W_{\text{adh}}}{3z_0}\left[\left(\frac{z_0}{z_{\text{tip}}+\mathrm{d}}\right)^3 - \left(\frac{z_0}{z_{\text{tip}}+d}\right)^9\right]\right\}2\pi r\mathrm{d}r \tag{3}$$

To evaluate this, z_{tip}, the vertical distance from the lowest point on the tip to other points on the tip is known from the TEM imaging and $F_{\text{tip/sample}}$ is calculated as a function of d. In this way, predicted force–distance curves can be calculated. The value of $F_{\text{pull-off}}$ is typically determined by the point of minimum force, except when this occurs at $d < z_0$; in these cases, $F_{\text{pull-off}} = F(d = z_0)$ as an approximation in order to avoid a computational singularity. The value of $d_{\text{snap-in}}$ is determined by the separation distance at which the gradient of the force curve is equal to the spring constant k_{lever} of the cantilever, i.e., $\left.\frac{\partial F_{\text{tip/sample}}}{\partial d}\right|_{\text{d}_{\text{snap-in}}} = k_{\text{lever}}$. The value of k_{lever} can be determined using a variety of methods [28].

Using the predetermined tip shape (as shown in Fig. 4a), we can numerically integrate the traction–separation relation (Eq. 3, shown in Fig. 4b) to calculate the tip/sample interaction force at every separation distance. From this tip/sample force–distance curve (Fig. 4(c)), we can calculate the predicted values of $F_{\text{pull-off}}$ and $d_{\text{snap-in}}$ that correspond to the input values of $W_{\text{adh,int}}$ and z_0.

3.2 Extracting $W_{\text{adh,int}}$ and z_0 from Known Values of $F_{\text{pull-off}}$ and $d_{\text{snap-in}}$

Above, $F_{\text{pull-off}}$ and $d_{\text{snap-in}}$ were calculated for input values of $W_{\text{adh,int}}$ and z_0. If experimental values have been determined for $F_{\text{pull-off}}$ and $d_{\text{snap-in}}$, then $W_{\text{adh,int}}$ and z_0 must be

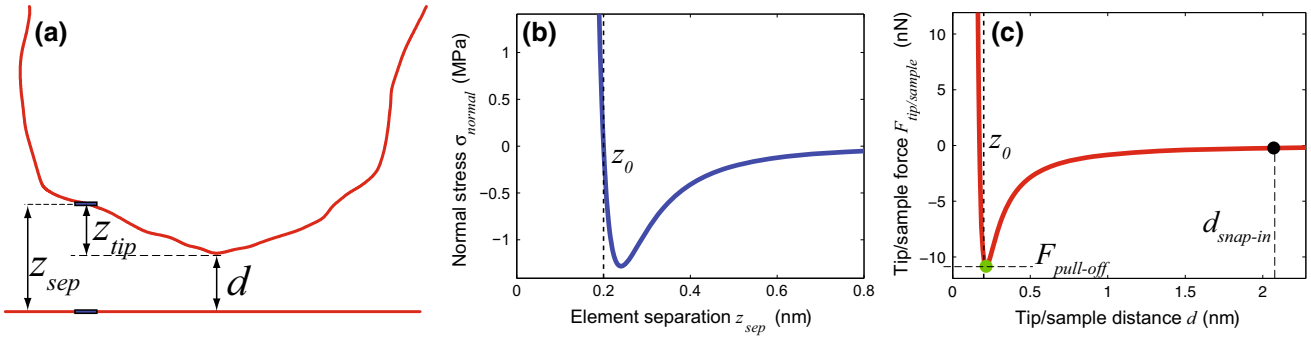

Fig. 4 Numerically, the traced tip profile (**a**) is broken into differential elements (indicated schematically with horizontal *black bars*), each of which has a separation from the surface equal to z_{sep}. The Lennard–Jones surface potential [Eq. 2, shown in (**b**) (with $W_{adh,int} = 0.25$ J/m^2, $z_0 = 0.2$ nm)] is applied to each element. As d is varied, the tip/sample interaction force $F_{tip/sample}$ can be calculated at each position (**c**). From these, the predicted pull-off force and snap-in distance can be calculated for each pair of values for ($W_{adh,int}$, z_0)

calculated. There is no analytical expression for extracting adhesion parameters ($W_{adh,int}$, z_0) from known values of $F_{pull\text{-}off}$ and $d_{snap\text{-}in}$. Rather, once values have been determined for $F_{pull\text{-}off}$ and $d_{snap\text{-}in}$, a search algorithm must be used to find best-fit values of $W_{adh,int}$ and z_0. To accomplish this, candidate values for ($F_{pull\text{-}off}$, $d_{snap\text{-}in}$) are calculated using a range of values for ($W_{adh,int}$, z_0)—typically $W_{adh,int} = [0.001,\ 1]$ J/m^2 and $z_0 = [0.05,\ 1.1]$ nm. The correct values of ($W_{adh,int}$, z_0) are chosen as those where the calculated values of ($F_{pull\text{-}off}$, $d_{snap\text{-}in}$) best match the input values. For general arbitrarily shaped tips, there will only be one specific pair of ($W_{adh,int}$, z_0) that make the predicted values of $F_{pull\text{-}off}$ and $d_{snap\text{-}in}$ match the experimental values; we take these parameters to be the correct values of $W_{adh,int}$ and z_0.

To clearly illustrate the method, an example is shown in Fig. 5 for a tip with arbitrarily chosen values of pull-off force and snap-in distance. Note that this is simulated data used for purposes of illustration only; to see the method applied to experimental data, refer to Ref. [24]. Using the tip profile from Fig. 2, force–distance curves, like those shown in Fig. 4c, were calculated for a variety of input pairs ($W_{adh,int}$, z_0). From these curves, values of pull-off force $F_{pull\text{-}off}$ and snap-in distance $d_{snap\text{-}in}$ were calculated for each input pair of ($W_{adh,int}$, z_0). These were compared against the chosen values of $F_{pull\text{-}off} = 5$ nN and $d_{snap\text{-}in} = 1.8$ nm (which otherwise would be measured in the experiment). Pull-off forces corresponding to a wide range of ($W_{adh,int}$, z_0) pairs are plotted in Fig. 5a. It is apparent that several different pairs of values can

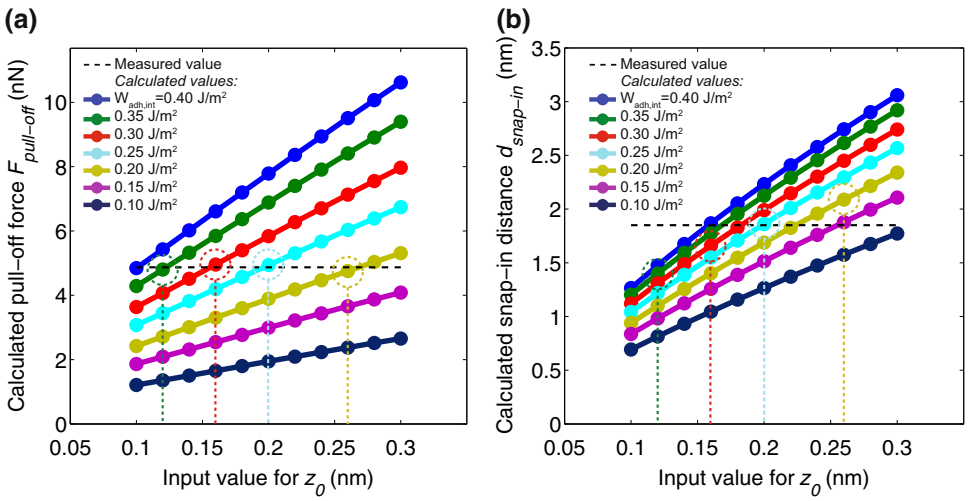

Fig. 5 The present method is demonstrated for a real tip (shown in Fig. 2) using artificially chosen values of pull-off force and snap-in distance. Pull-off force values for a wide range of ($W_{adh,int}$, z_0) pairs are shown in (**a**)—these are compared against the "measured" value of pull-off force (*black*, *dashed line*). It is apparent that the solution is not unique—the *four circles* indicate different possible pairs of ($W_{adh,int}$, z_0) that accurately predict this pull-off force for the given tip geometry. In (**b**), *circles* of corresponding color are calculated for the same four pairs of ($W_{adh,int}$, z_0) that were identified in (**a**). Three of the four *do not* match the snap-in distance, while the fourth *does*. Thus, in this example, $W_{adh,int} = 0.25$ J/m^2 and $z_0 = 0.2$ nm (Color figure online)

accurately describe the measured pull-off force. This demonstrates that $W_{adh,int}$ and z_0 cannot be simultaneously determined using pull-off force alone, as previously discussed. The novel aspect of the present method is that the snap-in distance is used as an independent measure of adhesion. Figure 5b shows the calculated snap-in distance for corresponding pairs of ($W_{adh,int}$, z_0). As shown, there is only one pair of values ($W_{adh,int}$, z_0) that accurately describes both pull-off force and snap-in distance. Note that since Fig. 5 is for demonstration purposes, only seven different values of $W_{adh,int}$ and eleven values of z_0 are shown; when this method is applied to real data, an automated algorithm is used to explore the $W_{adh,int} - z_0$ parameter space to find the best-fit values.

The first assumption of this method is that the tip is rigid, and therefore the tip shape is unchanged throughout the adhesion test. This renders the method equivalent to applying the so-called "Bradley limit" for spheres [12]; it applies for high-modulus materials and light loads (where the deformation due to strain is small). More specifically, this is expected to hold for bodies that are toward the DMT-like limit, where the adhesive attraction is assumed to not significantly distort the shape of the body. For spheres (mathematically modeled as paraboloids), a Maugis [8] parameter $\lambda < 0.1$ results in DMT-like behavior. Note that transition parameters exist for other geometries (such as Λ for power-law shapes) [13], but Grierson et al. show in Fig. 5 of [5] that the range of validity of the rigid approximation is similar for paraboloids (power-law exponent $n = 2$) and for other shapes ($n > 2$). Therefore, to assess the applicability of the present technique for any geometry, the Maugis parameter should be calculated (for instance, using the approach discussed in [20]) and should have a numerical value less than 0.1. Examples of materials where the present technique is expected to apply include metals and alloys, oxides, ceramics, inorganic semiconductors, and hard carbon coatings. The technique will not apply to biological materials or other soft materials such as soft polymers, elastomers, or hydrogels.

The second assumption of this method is that solid–solid adhesion is the primary contribution to total adhesion. When a water meniscus is present, it will add an additional adhesion force that is not explicitly accounted for here. In vacuum or an anhydrous environment, a capillary will not typically form. We also note that a meniscus is not automatically present when one works in ambient conditions. It has been shown that in some cases (e.g., with low-to-moderate relative humidities, and/or with hydrophobic materials), meniscus nucleation may not occur, and so solid–solid adhesion will determine the adhesive behavior (e.g., see Ref. [29]). In cases where a water meniscus does exist, the local geometry at the apex will play an important role and the present approach (high-resolution tip imaging, and recording of the snap-in and pull-out distances) could be further developed to help quantify how a meniscus contributes to adhesion.

4 Validation of the Method Using Simple Geometric Shapes and Quantification of Uncertainty

In the present section, two simple calculations are performed to validate the SNAP method. First, values of pull-off force $F_{pull\text{-}off}$ and snap-in distance $d_{snap\text{-}in}$ are calculated for simple geometric shapes assuming known values of the work of adhesion $W_{adh,int}$ and the range of adhesion z_0. This allows comparison of trends in results against prior literature and also illuminates advantages and disadvantages of the method. Second, using only knowledge of the tip shape and the values of $F_{pull\text{-}off}$ and $d_{snap\text{-}in}$ calculated above, the $W_{adh,int}$ and z_0 values are extracted using the search algorithm to verify that extracted values match the input values of $W_{adh,int}$ and z_0 used above. The latter calculation serves both as a check of self-consistency and also a quantification of uncertainty in the method.

4.1 Calculating Tip/Sample Force–Distance Curves Using Probes with Simple Geometric Shapes

Force–distance curves were computed for three different reference tips with shapes described by three simple analytical functions: a cylindrical flat punch; a paraboloid (i.e., a two-dimensional parabola that has been revolved about its central axis); and a right cone. The three shapes are shown in Fig. 6 and can be mathematically represented using power-law functions with exponents of $n \to \infty$, $n = 2$, and $n = 1$, respectively. The widths of these tips were chosen to achieve values of $F_{pull\text{-}off}$ that were similar and realistic (50–70 nN) for mid-range adhesion parameters, i.e., $W_{adh,int} = 0.55$ J/m^2 and $z_0 = 0.5$ nm. This yielded a flat punch of end radius 4 nm; a paraboloid defined [12] by $z_{tip} = r^2/(2R_{tip})$ with $R_{tip} = 20$ nm; and a right cone with an opening half-angle of 84°.

These shapes were chosen as they represent extremes of tip shape. The flat punch represents the bluntest possible tip. The force–distance curve for this tip represents the form of the underlying Lennard–Jones surface potential (differing only by a constant representing the surface area of the punch). The paraboloid was chosen as it is used in many contact mechanics models as an approximation for a sphere [12]. It represents an intermediate level of sharpness between a flat punch and a cone. The right cone represents the extreme of the sharpest possible probe, converging to a single point at the apex. This unphysically sharp analytical shape is useful for demonstrating trends and also motivates

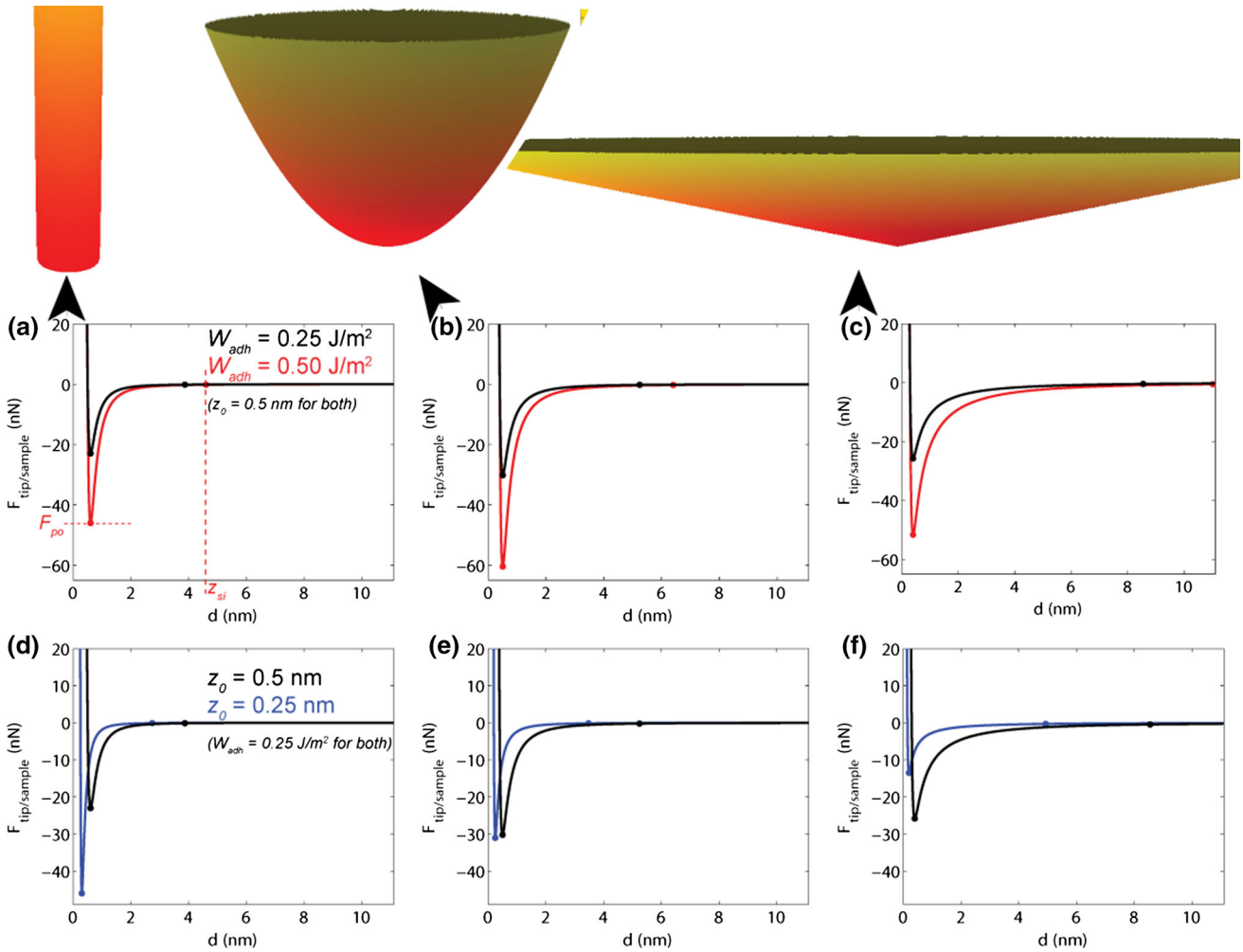

Fig. 6 Force–distance curves were calculated for simple, geometric shapes (shown at *top*): a flat circular punch (*left column*); a paraboloid (*center column*); and a *right cone* (*right column*). Here, the tip/sample interaction force is calculated over a range of tip positions d, with the flat substrate located at $d = 0$. These force–distance curves are shown (**a**–**c**) for two different values of the work of adhesion ($W_{\text{adh,int}} = 0.25$, 0.50 J/m^2) at a constant value of range of adhesion ($z_0 = 0.5$ nm). In (**d**–**f**), force curves are compared for two different ranges of adhesion ($z_0 = 0.25$, 0.5 nm) and a constant work of adhesion ($W_{\text{adh,int}} = 0.25$ J/m^2). The points on the curves corresponding to pull-off and snap-in are labeled in each plot with circular points assuming a cantilever spring constant of 0.1 N/m; values of pull-off force ($F_{\text{pull-off}}$) and snap-in distance ($d_{\text{snap-in}}$) are explicitly indicated in (**a**). Note that the legends in the *left-most panels* apply for *all panels* in that *row*

one of the constraints imposed on the present method. Figure 6 shows the force–distance curves for each shape, calculated using the parameters ($W_{\text{adh,int}} = 0.25$ and 0.50 J/m^2, $z_0 = 0.25$ and 0.5 nm), with snap-in distances and pull-off forces indicated for a spring constant of $k = 0.1$ N/m. These plots are included to show the effects of $W_{\text{adh,int}}$ and z_0, and the differences in behavior for each shape.

The dependence of pull-off and snap-in on the range of adhesion z_0 is more complex and depends strongly on the geometry of the tip. However, all trends shown here can be compared with recent publications [5, 13] discussing adhesion of tips with power-law profiles. For a flat punch interacting with a flat surface through a Lennard–Jones surface potential, the pull-off force decreases as z_0 is increased. As noted above, a flat punch tip is equivalent to a power-law shape with a very large power exponent ($n \to \infty$). The trend found here, of decreasing adhesive force with increasing z_0 for constant $W_{\text{adh,int}}$, agrees with the trend shown in Grierson et al. [5]. for all shapes with power-law exponent $n > 2$. By contrast, for the parabolic tip (a power-law shape where the power exponent $n = 2$), the pull-off force is independent of z_0. This agrees not only with trends from Refs. [13, 20], but also with the predictions of the Maugis-Dugdale model [8]. The pull-off force agrees exactly with the prediction of the Bradley limit [12] for rigid spheres and that of the DMT model: [12], namely that the pull-off force is equal to $2\pi R_{tip} W_{\text{adh,int}}$. Finally, for

Table 1 In order to check self-consistency and estimate uncertainty, the following test was run: First, a range of values for $W_{adh,int}$ and z_0 were chosen (columns 2, 3); second, $F_{pull\text{-}off}$ and $d_{snap\text{-}in}$ were calculated for a variety of tip shapes (columns 4, 5); third, reasonable uncertainty was added to those calculated values of $F_{pull\text{-}off}$, $d_{snap\text{-}in}$ (columns 6, 7), then values of $W_{adh,int}$ and z_0 were extracted (columns 8, 9)

Tip shape description	Input $W_{adh,int}$ (mJ/m^2)	Input z_0 (nm)	Calc. F_{po} (nN)	Calc. d_{si} (nm)	Input F_{po} (nN)	Input d_{si} (nm)	Calc. $W_{adh,int}$ (mJ/m^2)	Calc. z_0 (nm)
Flat punch (4.0 nm end radius)	0.55	0.50	51	4.7	51 ± 2.6	4.7 ± 0.23	0.54 ± 0.04	0.50 ± 0.03
	0.55	0.15	169	2.6	169 ± 8.5	2.6 ± 0.23	0.54 ± 0.06	0.15 ± 0.02
	0.55	1.00	26	6.7	26 ± 1.3	6.7 ± 0.23	0.54 ± 0.02	1.0 ± 0.05
	0.10	0.50	9.3	3.1	9.3 ± 0.5	3.1 ± 0.23	0.10 ± 0.01	0.50 ± 0.05
	1.0	0.50	93	5.5	93 ± 4.7	5.5 ± 0.23	0.99 ± 0.06	0.50 ± 0.03
Paraboloid (20 nm radius)	0.55	0.50	69	7.7	69 ± 3.4	7.7 ± 0.23	0.55 ± 0.04	0.50 ± 0.03
	0.55	0.15	68	3.4	68 ± 3.4	3.4 ± 0.23	0.56 ± 0.04	0.15 ± 0.02
	0.55	1.00	69	12	69 ± 3.4	12 ± 0.23	0.55 ± 0.02	1.0 ± 0.03
	0.10	0.50	13	4.4	13 ± 0.62	4.4 ± 0.23	0.1 ± 0.01	0.50 ± 0.04
	1.0	0.50	125	9.4	125 ± 6.3	9.4 ± 0.23	1.0 ± 0.06	0.50 ± 0.02
Right cone (84° opening half-angle)	0.55	0.50	54	16	54 ± 2.7	16 ± 0.23	0.56 ± 0.06	0.50 ± 0.02
	0.55	0.15	16	5.0	16 ± 0.8	5.0 ± 0.23	0.57 ± 0.07	0.15 ± 0.01
	0.55	1.00	106	28	105 ± 5.3	28 ± 0.23	0.56 ± 0.05	0.99 ± 0.05
	0.10	0.50	9.8	7.1	9.8 ± 0.5	7.1 ± 0.23	0.10 ± 0.01	0.50 ± 0.03
	1.0	0.50	98	20.4	98 ± 4.9	20 ± 0.23	1.0 ± 0.12	0.50 ± 0.03
Real tip Fig. 2	0.55	0.50	81	8.4	81 ± 4.1	8.4 ± 0.23	0.56 ± 0.04	0.50 ± 0.02
	0.55	0.15	63	3.8	63 ± 3.2	3.8 ± 0.23	0.56 ± 0.04	0.15 ± 0.02
	0.55	1.0	88	4.4	88 ± 13	4.4 ± 0.23	0.56 ± 0.04	0.99 ± 0.04
	0.10	0.50	15	4.8	15 ± 0.7	4.8 ± 0.23	0.10 ± 0.01	0.50 ± 0.04
	1.0	0.50	148	10	148 ± 7.4	10 ± 0.23	0.99 ± 0.06	0.50 ± 0.02

the conical shape, the pull-off force *increases* as z_0 is increased for a constant $W_{adh,int}$. This trend for a conical shape (a power-law shape where the power exponent $n = 1$) is in agreement with the so-called DMT-n limit described by Zheng and Yu [13].

In summary, for the probe shapes shown in Fig. 6 and other shapes tested (not shown), consistent trends of behavior hold: For shapes blunter than a paraboloid ($n > 2$), the pull-off force decreases as z_0 increases; for shapes sharper than a paraboloid ($n < 2$), the pull-off force increases with z_0; and for a paraboloid ($n = 2$), the pull-off force is unaffected by changes in z_0. (Note that, for rigid tips, the JKR limit (with its modified pull-off force) is not reached.)

The dependence of pull-off force on adhesive range can be understood as a competition between two factors: as the range of adhesion is increased for a constant work of adhesion, a larger section of the probe contributes to the adhesive interaction, but the adhesive stress at a given separation distance is decreased. This can be visualized in Fig. 4b, where an increase in z_0 stretches the curve along the x-axis; in order to maintain a constant integrated area ($W_{adh,int}$), the strength of the interaction at a given separation (shown on the y-axis) must be decreased. The "winner" of this competition depends on the geometry of the body. For blunt shapes with steep sidewalls—like a punch—an increase in z_0 decreases the pull-off force. This is because relatively little additional material is interacting due to the increased range of adhesion; instead, the primary effect is simply to reduce the adhesive stress on the material in close proximity. By contrast, for tapered shapes—like a cone—the increase in material that is interacting overwhelms the weakening of the adhesive stress and an increase in z_0 leads to a larger pull-off force. A parabola represents the shape where these competing effects exactly balance, regardless of the chosen traction–separation relation [21]. In this case, the pull-off force depends only on the work of adhesion $W_{adh,int}$.

Another important result emerges from Fig. 6: Without some modification, a simple integration of the Lennard–Jones surface potential leads to an unphysical result for ultra-sharp tips when the finite rigidity and strength of the materials are considered. Specifically, for the punch and parabola shapes in Fig. 6, the separation distance corresponding to the minimum force ($F_{pull\text{-}off}$) is equal to or larger than the equilibrium flat-on-flat separation z_0. However, for the cone shape, the separation at $F_{pull\text{-}off}$ is smaller than z_0. Note that z_0 rigorously designates the

equilibrium separation of *surface area elements*, but is not the same as the equilibrium separation of tip and sample. For a very sharp shape, this could lead to high compressive stress in the closest elements—which are not accommodated in the present method in which the bodies are assumed to be rigid. To eliminate the unphysically large Lennard–Jones stresses on the tip apex, an additional constraint was added to the method: In calculating the pull-off force, the tip-sample minimum separation distance is not allowed to fall below the value of z_0 chosen for that simulation (i.e., $d \geq z_0$). This simple constraint introduces hard-wall repulsion when the minimum separation of the bodies is z_0. This avoids resorting to a much more complex and time-consuming analysis that takes elasticity and plasticity into account, such as in Ref. [30].

4.2 Extracting Adhesion Parameters Using Standard Geometric Shapes: Checking Self-consistency and Quantifying the Uncertainty

Above, values of $F_{\text{pull-off}}$ and $d_{\text{snap-in}}$ were calculated for standard geometric shapes using specified typical adhesion parameters (i.e., $W_{\text{adh,int}} = 0.3$ or 0.6 J/m^2 and $z_0 = 0.1$ or 0.3 nm). Here, the self-consistency of the method is checked along with its uncertainty. For calculating the uncertainty of the present method, a simple propagation of uncertainty cannot be used since analytical expressions do not exist. Instead, values for ($W_{\text{adh,int}}$, z_0) were calculated after the addition of reasonable uncertainty to the input values of $F_{\text{pull-off}}$ and $d_{\text{snap-in}}$.

First, $F_{\text{pull-off}}$ and $d_{\text{snap-in}}$ were calculated for a wide range of possible adhesion parameters ($W_{\text{adh,int}} = \{0.1, 0.55, 1.0\}$ J/m^2 and $z_0 = \{0.15, 0.5, 1.0\}$ nm) for the three geometric shapes discussed above and for a real tip. Then, uncertainty was added to these calculated values of $F_{\text{pull-off}}$ and $d_{\text{snap-in}}$: ± 5 % for $F_{\text{pull-off}}$ due to uncertainties in calibration of the cantilever spring constant [28] and $\pm$ 0.23 nm for $d_{\text{snap-in}}$ as an upper bound on the accuracy of height measurements in an AFM [28] or TEM [31]. Then, these values—with uncertainty—were used to extract a range of $W_{\text{adh,int}}$ and z_0 for each case. All results are reported in Table 1. The maximum variation in calculated values is reported in the final columns of Table 1, as an uncertainty of the "calculated" $W_{\text{adh,int}}$ and z_0. It is demonstrated that, for a wide range of adhesion values and tip shapes, the uncertainty of the method is typically less than 10 % for both $W_{\text{adh,int}}$ and z_0, and up to 12 % in certain cases.

The primary conclusion from the calculations in this section is that the present technique works well for a wide range of shapes and physical parameters. The method is self-consistent, and the trends in the results agree with previously published reports investigating adhesion of probes with standard shapes defined by analytical functions. These results demonstrate that the pull-off force and snap-in distance depend on the work of adhesion and range of adhesion in significantly different ways for different classes of tip geometry. Further, using reasonable values, the uncertainty in the present method for determining $W_{\text{adh,int}}$ and z_0 from measurements of $F_{\text{pull-off}}$ and $d_{\text{snap-in}}$ is estimated to be less than 12 % for both values.

5 Conclusions

A current limitation in prediction of adhesive forces stems from a lack of reliable data for the intrinsic work of adhesion $W_{\text{adh,int}}$ and, even more so, for the range of adhesion z_0 for a given pair of materials. The novel advancement of the present method is to introduce a technique for simultaneously measuring these two parameters for effectively rigid materials. This technique requires knowledge of the tip shape (which can be measured using a number of techniques) and measurement of the pull-off force and snap-in distance (both of which can be easily measured in an AFM adhesion test). Then the experimental data can be fit to the model to extract $W_{\text{adh,int}}$ and z_0. The method has been validated analytically using simple geometric shapes and is found to be self-consistent, reproducing trends in behavior established in previous numerical and simulation studies. The uncertainty in the technique has been estimated at no more than 12 % for a wide range of reasonable geometric and physical parameters, and is typically less than 10 %. Overall, the method is widely applicable for characterizing the adhesion parameters between a variety of material pairs, as shown, for example, for a silicon/diamond interface [24].

Acknowledgments The authors acknowledge useful discussions with K. Turner and D. Grierson. R.W.C and T.D.B.J. acknowledge support from National Science Foundation under award No. CMMI12-00093. R.W.C., T.D.B.J., and J.A.L. acknowledge support from the UPenn MRSEC Program of the National Science Foundation under award No. DMR11-20901. R.W.C acknowledges support from AFOSR under Contract No. FA2386-14-1-4071 AOARD.

References

1. Persson, B.: Adhesion between elastic bodies with randomly rough surfaces. Phys. Rev. Lett. **89**, 245502 (2002)
2. Mastrangelo, C.H., Hsu, C.H.: A simple experimental technique for the measurement of the work of adhesion of microstructures. 5th Technical Digest, IEEE Solid–State Sensor and Actuator Workshop, pp. 208–212 (1992)
3. Greenwood, J.A.: Adhesion of small spheres. Philos. Mag. **89**, 945–965 (2009)

4. Yao, H., Ciavarella, M., Gao, H.: Adhesion maps of spheres corrected for strength limit. J. Colloid Interface Sci. **315**, 786–790 (2007)
5. Grierson, D.S., Liu, J., Carpick, R.W., Turner, K.T.: Adhesion of nanoscale asperities with power-law profiles. J. Mech. Phys. Solids **61**, 597–610 (2013)
6. Feng, J.Q.: Adhesive contact of elastically deformable spheres: a computational study of pull-off force and contact radius. J. Colloid Interface Sci. **238**, 318–323 (2001)
7. Israelachvili, J.N.: Intermolecular and Surface Forces. Academic Press, San Francisco, CA (2011)
8. Maugis, D.: Adhesion of spheres: the JKR-DMT transition using a Dugdale model. J. Colloid Interface Sci. **150**, 243–269 (1992)
9. Pastewka, L., Robbins, M.O.: Contact between rough surfaces and a criterion for macroscopic adhesion. Proc. Natl. Acad. Sci. **111**, 3298–3303 (2014)
10. Barthel, E.: On the description of the adhesive contact of spheres with arbitrary interaction potentials. J. Colloid Interface Sci. **200**, 7–18 (1998)
11. Mulakaluri, N., Persson, B.: Adhesion between elastic solids with randomly rough surfaces: comparison of analytical theory with molecular-dynamics simulations. EPL (Europhysics Letters). 96, 66003 (2011)
12. Johnson, K.L.: Contact Mechanics. Cambridge University Press, Cambridge (2011)
13. Zheng, Z., Yu, J.: Using the Dugdale approximation to match a specific interaction in the adhesive contact of elastic objects. J. Colloid Interface Sci. **310**, 27–34 (2007)
14. Yu, N., Polycarpou, A.A.: Adhesive contact based on the Lennard–Jones potential: a correction to the value of the equilibrium distance as used in the potential. J. Colloid Interface Sci. **278**, 428–435 (2004)
15. Jarvis, S.P., Oral, A., Weihs, T.P., Pethica, J.B.: A novel force microscope and point contact probe. Rev. Sci. Instrum. **64**, 3515 (1993)
16. Jarvis, S.P., Yamada, H., Yamamoto S.-I., Tokumoto, H.: A new force controlled atomic force microscope for use in ultrahigh vacuum. Rev. Sci. Instrum. **67**, 2281 (1996)
17. Ashby, P.D., Chen, L.W., Lieber, C.M.: Probing intermolecular forces and potentials with magnetic feedback chemical force microscopy. J. Am. Chem. Soc. **122**, 9467 (2000)
18. Giessibl, F.J.: Advances in atomic force microscopy. Rev. Mod. Phys. **75**, 949–983 (2003)
19. Joyce, S.A., Houston, J.E.: A new force sensor incorporating force-feedback control for interfacial force microscopy. Rev. Sci. Instrum. **62**, 710 (1991)
20. Grierson, D., Flater, E., Carpick, R.: Accounting for the JKR-DMT transition in adhesion and friction measurements with atomic force microscopy. J. Adhes. Sci. Technol. **19**, 291–311 (2005)
21. Greenwood, J.: Adhesion of elastic spheres. Proc. Roy. Soc. A **453**, 1277–1297 (1997)
22. Tabor, D.: Surface forces and surface interactions. J. Colloid Interface Sci. **58**, 2–13 (1977)
23. Persson, B.: Nanoadhesion. Wear **254**, 832–834 (2003)
24. Jacobs, T.D.B., Lefever, J.A., Carpick, R.W.: Measurement of the length and strength of adhesive interactions in a nanoscale silicon-diamond interface. Adv. Mater. Interfaces (2015). doi:10.1002/admi.201400547
25. Chung, K., Lee, Y., Kim, D.: Characteristics of fracture during the approach process and wear mechanism of a silicon AFM tip. Ultramicroscopy **102**, 161–171 (2005)
26. Liu, J., Notbohm, J.K., Carpick, R.W., Turner, K.T.: Method for characterizing nanoscale wear of atomic force microscope tips. ACS Nano **4**, 3763–3772 (2010)
27. Cappella, B., Dietler, G.: Force-distance curves by atomic force microscopy. Surf. Sci. Rep. **34**, 1–104 (1999)
28. Ohler, B.: Cantilever spring constant calibration using laser Doppler vibrometry. Rev. Sci. Instrum. **78**, 063701 (2007)
29. Greiner, C., Felts, J.R., Dai, Z., King, W.P., Carpick, R.W.: Controlling nanoscale friction through the competition between capillary adsorption and thermally activated sliding. ACS Nano **6**, 4305–4313 (2012)
30. Hui, C.-Y., Long, R.: Direct extraction of work of adhesion from contact experiments: generalization of JKR theory to flexible structures and large deformation. J Adhes. **88**, 70–85 (2012)
31. Jacobs, T.D.B., Ryan, K.E., Keating, P.L., Grierson, D.S., Lefever, J.A., Turner, K.T., Harrison, J.A., Carpick, R.W.: The effect of atomic-scale roughness on the adhesion of nanoscale asperities: a combined simulation and experimental investigation. Tribol. Lett. **50**, 81–93 (2013)